Related Commentary, page 4996

Research article

ADCK4 mutations promote steroid-resistant nephrotic syndrome through CoQ_{10} biosynthesis disruption

Shazia Ashraf,[1] Heon Yung Gee,[1] Stephanie Woerner,[2,3] Letian X. Xie,[4] Virginia Vega-Warner,[5] Svjetlana Lovric,[1] Humphrey Fang,[1] Xuewen Song,[6] Daniel C. Cattran,[6] Carmen Avila-Casado,[7] Andrew D. Paterson,[8] Patrick Nitschké,[9] Christine Bole-Feysot,[10] Pierre Cochat,[11] Julian Esteve-Rudd,[12] Birgit Haberberger,[13,14] Susan J. Allen,[5] Weibin Zhou,[5] Rannar Airik,[1] Edgar A. Otto,[5] Moumita Barua,[15] Mohamed H. Al-Hamed,[16] Jameela A. Kari,[17] Jonathan Evans,[18] Agnieszka Bierzynska,[19] Moin A. Saleem,[19] Detlef Böckenhauer,[20] Robert Kleta,[20] Sherif El Desoky,[17] Duygu O. Hacihamdioglu,[21] Faysal Gok,[21] Joseph Washburn,[22] Roger C. Wiggins,[23] Murim Choi,[24,25] Richard P. Lifton,[24,25] Shawn Levy,[26] Zhe Han,[27] Leonardo Salviati,[28] Holger Prokisch,[13,14] David S. Williams,[12] Martin Pollak,[11] Catherine F. Clarke,[4] York Pei,[6] Corinne Antignac,[2,3,29] and Friedhelm Hildebrandt[1,30,31]

[1]Division of Nephrology, Department of Medicine, Boston Children's Hospital, Harvard Medical School, Boston, Massachusetts, USA. [2]Inserm U983, Necker Hospital, Paris, France. [3]Université Paris Descartes, Sorbonne Paris Cité, Imagine Institute, Paris, France. [4]Department of Chemistry and Biochemistry and Molecular Biology Institute, UCLA, Los Angeles, California, USA. [5]Department of Pediatrics, University of Michigan, Ann Arbor, Michigan, USA. [6]Division of Nephrology, University Health Network, and University of Toronto, Toronto, Ontario, Canada. [7]Department of Pathology, University Health Network, Toronto, Ontario, Canada. [8]Program in Genomic Biology, Hospital for Sick Children, Toronto, Ontario, Canada. [9]Bioinformatics Plateform, Université Paris Descartes, Paris, France. [10]Genomics Plateform, Imagine Institute, Université Paris Descartes, Paris, France. [11]Service de Néphrologie et Rhumatologie Pédiatrique, Centre de référence des maladies rénales rares, Hôpital Femme Mère Enfant, Hospices Civils de Lyon, Bron, France. [12]Jules Stein Eye Institute, UCLA School of Medicine, Los Angeles, California, USA. [13]Institute of Human Genetics, Helmholtz Zentrum Munich, Neuherberg, Germany. [14]Institute of Human Genetics, Klinikum rechts der Isar, Technical University Munich, Munich, Germany. [15]Division of Nephrology, Department of Medicine, Beth Israel Deaconess Medical Center, Boston, Massachusetts, USA. [16]Institute of Genetic Medicine, Newcastle University, Central Parkway, Newcastle upon Tyne, United Kingdom. [17]Pediatrics Department, King Abdulaziz University, Jeddah, Kingdom of Saudi Arabia. [18]Nottingham University Hospitals, Nottingham, United Kingdom. [19]Children's and Academic Renal Unit, University of Bristol, Bristol, United Kingdom. [20]UCL Institute of Child Health and Paediatric Nephrology, Great Ormond Street Hospital, London, United Kingdom. [21]Department of Pediatric Nephrology and Rheumatology, Gülhane Military Academy of Medicine, School of Medicine, Etlik, Ankara, Turkey. [22]Biomedical Research Core Facilities and [23]Department of Internal Medicine, Department of Pathology, and Department of Otolaryngology, University of Michigan, Ann Arbor, Michigan, USA. [24]Department of Genetics, Howard Hughes Medical Institute, and [25]Yale Center for Mendelian Genomics, Yale University School of Medicine, New Haven, Connecticut, USA. [26]HudsonAlpha Institute for Biotechnology, Huntsville, Alabama, USA. [27]Department of Internal Medicine — Molecular Medicine and Genetics, University of Michigan, Ann Arbor, Michigan, USA. [28]Department of Woman and Child Health, University of Padova and Istituto di Ricerca Pediatrica Città della Speranza, Padova, Italy. [29]Assistance Publique – Hôpitaux de Paris, Department of Genetics, Necker Hospital, Paris, France. [30]Department of Human Genetics, University of Michigan, Ann Arbor, Michigan, USA. [31]Howard Hughes Medical Institute, Chevy Chase, Maryland, USA.

Identification of single-gene causes of steroid-resistant nephrotic syndrome (SRNS) has furthered the understanding of the pathogenesis of this disease. Here, using a combination of homozygosity mapping and whole human exome resequencing, we identified mutations in the aarF domain containing kinase 4 (*ADCK4*) gene in 15 individuals with SRNS from 8 unrelated families. ADCK4 was highly similar to ADCK3, which has been shown to participate in coenzyme Q_{10} (CoQ_{10}) biosynthesis. Mutations in *ADCK4* resulted in reduced CoQ_{10} levels and reduced mitochondrial respiratory enzyme activity in cells isolated from individuals with SRNS and transformed lymphoblasts. Knockdown of *adck4* in zebrafish and *Drosophila* recapitulated nephrotic syndrome-associated phenotypes. Furthermore, ADCK4 was expressed in glomerular podocytes and partially localized to podocyte mitochondria and foot processes in rat kidneys and cultured human podocytes. In human podocytes, ADCK4 interacted with members of the CoQ_{10} biosynthesis pathway, including COQ6, which has been linked with SRNS and COQ7. Knockdown of ADCK4 in podocytes resulted in decreased migration, which was reversed by CoQ_{10} addition. Interestingly, a patient with SRNS with a homozygous *ADCK4* frameshift mutation had partial remission following CoQ_{10} treatment. These data indicate that individuals with SRNS with mutations in *ADCK4* or other genes that participate in CoQ_{10} biosynthesis may be treatable with CoQ_{10}.

Introduction

Nephrotic syndrome (NS) is a chronic kidney disease that is defined by significant proteinuria (>40 mg/m^2/h), with resulting hypoalbuminemia, which causes edema (1). NS constitutes the second most frequent cause of end-stage kidney disease (ESKD)

Authorship note: Shazia Ashraf and Heon Yung Gee contributed equally to this work.

Conflict of interest: The authors have declared that no conflict of interest exists.

Citation for this article: *J Clin Invest.* 2013;123(12):5179–5189. doi:10.1172/JCI69000.

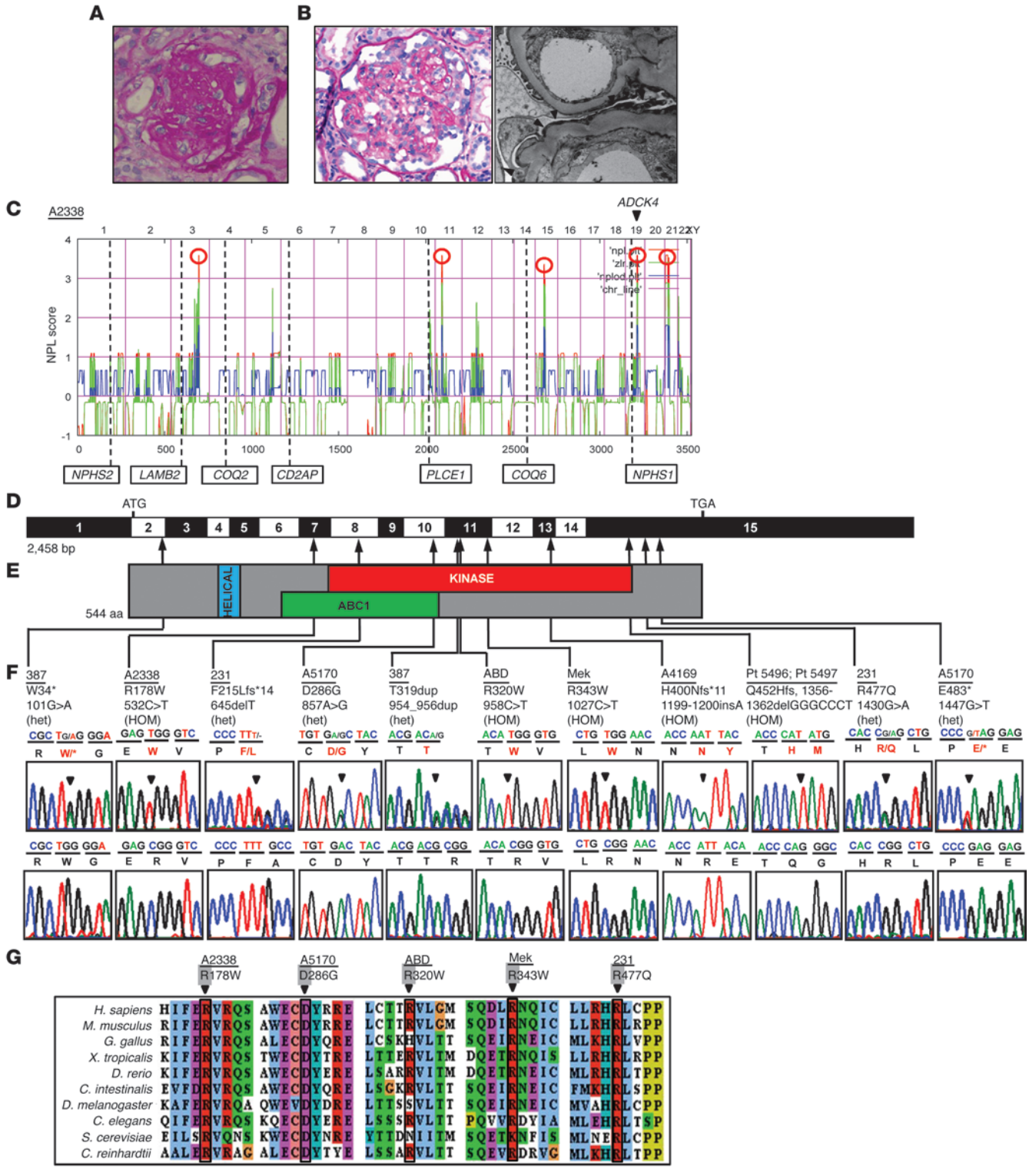

Figure 1
HM and exon capture resequencing reveal *ADCK4* mutations as causes of SRNS. (**A**) Renal histology of individual A2338-21 reveals global glomerulosclerosis by excess PAS staining (red). Original magnification, ×200. (**B**) Renal histology of individual Pt5496 shows cFSGS. PAS staining (left) reveals retraction and collapse of the capillary tuft, with numerous foam cells and groups of hyperplastic and vacuolated visceral epithelial cells. Original magnification, ×40. Electron microscopy image (right) shows foot process effacement (black arrowheads). In addition, capillary basement membranes are thickened and remodeled. Original magnification, ×15,000. (**C**) Nonparametric LOD (log of the odds ratio) (NPL) score profile across the human genome in 2 siblings with SRNS of consanguineous family A2338. Five maximum NPL peaks (red circles) indicate candidate regions of homozygosity by descent. *ADCK4* is positioned (arrowhead) within a peak on chromosome (Chr) 19. Numbers at the bottom of the panels are measured in centimorgan (cM). (**D**) Exon structure of human *ADCK4* cDNA. *ADCK4* contains 15 exons. Positions of start codon (ATG) and of stop codon (TGA) are indicated. (**E**) Domain structure of ADCK4. The helical, ABC1, and kinase domains are depicted by colored bars in relation to encoding exon position. (**F**) Eleven different *ADCK4* mutations in eight families with SRNS. Family numbers and amino acid changes (Table 1) are given above sequence traces. Arrowheads denote altered nucleotides. Lines and arrows indicate positions of mutations in relation to exon D and protein domain E. (**G**) For the 5 missense mutations (p.R178W, p.D286G, p.R320W, p.R343W, and p.R477Q) conservation across evolution of altered amino acid residues is shown.

in children (2, 3). While most children with NS have steroid-sensitive NS, approximately 10%–20% of children and 40% of adults with NS do not achieve sustained remission after glucocorticoid therapy and additional immunosuppressive therapy and enter into ESKD (1). These cases of steroid-resistant NS (SRNS) manifest histologically as focal segmental glomerulosclerosis (FSGS) (4).

Recent discoveries of the single-gene causes of NS have significantly increased our understanding of glomerular filtration barrier physiology and of pathogenic mechanisms of NS (1). To date, more than 9 recessive genes that cause NS if mutated have been identified (5, 6). Overall, these genes account for up to approximately 66% of NS that starts within the first year of life (2). However, monogenic causes of a significant proportion of childhood- or adult-onset NS are still molecularly unsolved. Moreover, recently identified genes are very rare, being mutated in only one family out of hundreds (7). To overcome the limitations posed by the rarity of genes when identifying genes associated with NS, we established a strategy of combining homozygosity mapping (HM) with whole-exome resequencing (WER) (8, 9). Here, we applied this approach to sibling cases of childhood-onset NS and thereby identified mutations of aarF domain containing kinase 4 (*ADCK4*) as a single-gene cause of SRNS.

Results

Mutations in ADCK4 cause SRNS. To identify further single-gene causes of SRNS, we performed HM followed by WER in a group of individuals with histology that revealed FSGS (Figure 1, A and B). In a family (A2338) of Arab origin, 2 siblings had early-onset SRNS and renal histology that revealed glomerulosclerosis (Figure 1A). HM in both affected siblings yielded 5 regions of homozygosity by descent with a cumulative genomic length of approximately 115 Mb, none of which coincided with any of 7 common recessive causes of SRNS (Figure 1C). The presence of homozygosity strongly suggested a recessive causative gene, and the lack of overlap with known NS gene loci suggested that the gene to be identified in this family would be novel. By WER in one of the affected siblings from family A2338, we detected a homozygous missense mutation (c.532C>T;p.R178W) in *ADCK4* (NM_024876.3) on chromosome 19, encoding ADCK4. This variant was the only homozygous variant remaining from the variant filtering process (Supplemental Table 1; supplemental material available online with this article; doi:10.1172/JCI69000DS1). The mutation (p.R178W) alters an amino acid residue conserved throughout evolution from *Chlamydomonas reinhardtii*. It segregated with the affected status in this family and was absent from >190 ethnically matched healthy control individuals and from >8,600 European controls in the Exome Variant Server (http://evs.gs.washington.edu/EVS/).

WER in an addtional 6 different families with SRNS also yielded 9 additional mutations in *ADCK4* (3 families with homozygous mutations and 3 families with compound heterozygous mutations) (Figure 1, D–G, and Table 1). WER of one affected individual in family 386 identified compound heterozygous mutations: c.101G>A;p.W34* and c.954_956dup;p.T319dup. We identified compound heterozygous mutations (c.645delT;p.F215Lfs*14 and c.4130G>A;p.R477Q in *ADCK4*) in 2 affected siblings from family 231 from Algeria (Figure 1F and Table 1). The missense mutation (p.R477Q) altered an amino acid residue that was continually conserved from *C. reinhardtii* to humans (Figure 1G). In a family (A5170) of 3 affected siblings, WER revealed compound heterozygous mutations: c.857A>G;p.D286G and c.1447G>T;p.E483* in *ADCK4* (Figure 1F and Table 1). This missense mutation (p.D286G) altered an amino acid residue that is continually conserved from *C. reinhardtii* to humans (Figure 1G). One of the homozygous mutations (p.R320W) in *ADCK4* was found in 2 affected siblings from the ABD family from Tunisia in an amino acid residue continually conserved throughout evolution from *C. reinhardtii* (Figure 1, F and G, and Table 1). In another family (Mek) from Morocco, we discovered a missense mutation c.1027C>T;p.R343W in this gene in 2 affected siblings (Figure 1F and Table 1). The amino acid residue R343 has been conserved from *C. reinhardtii* to humans (Figure 1G). The other homozygous mutation was an out-of-frame deletion of 7 bases (p.Q452Hfs) in exon 15 of *ADCK4* in 2 affected siblings from a family from India, with renal histology showing collapsing FSGS (cFSGS) (Figure 1F and Table 1).

To discover additional mutations in *ADCK4*, we then performed multiplex barcoded array-based PCR amplification and next-generation sequencing in an additional 400 individuals with SRNS (10). In an individual with SRNS (A4169-21), we detected a homozygous insertion of an "A" (H400Nfs*11) in exon 13 of *ADCK4* (Figure 1F and Table 1). Sequences of primers used to amplify exons and exon-intron boundaries of *ADCK4* are listed in Supplemental Table 2. All 15 affected individuals of the 8 families with recessive mutations in *ADCK4* had SRNS. Renal biopsy revealed FSGS in most cases. Interestingly, in 3 affected individuals (1146, Pt5497, and Pt5497), renal histology showed cFSGS (Figure 1B and Table 1). Moreover, the individual A4169-21, who has a homozygous truncating allele, showed the earliest onset of SRNS and also presented with developmental delay (Table 1).

ADCK4 spans 12 kb on chromosome 19q13.1. Up to 17 different putative alternatively spliced *ADCK4* transcripts encoding different proteins have been proposed (AceView; http://www.ncbi.nlm.nih.gov/ieb/research/acembly/index.html). The longest transcript of *ADCK4* (NM_024876.3) has 14 coding exons (Figure 1D) and encodes a 60.1-kDa protein (NP_079152.3, isoform a, 544

Table 1
Recessive *ADCK4* mutations detected in individuals with SRNS

Family–individual	Ethnic origin	Parental consanguinity	Nucleotide alteration(s)[A]	Alteration(s) in coding sequence	Exon (segregation)	Amino acid sequence conservation	Age at onset	Kidney disease	Age at ESKD	Treatment and renal transplantation	Histology (at age)	Extrarenal manifestations
387	European	No	c.101G>A	p.W34*	2 (het, ND)	NA						
387–21			c.954_956dup	pT319dup	11 (het, ND)	NA	10 yr	SRNS	12 yr	PNL, tacrolimus, first transplant (14 yr)	FSGS (10 yr)	No
A2338	Arab	Yes	c.532C>T	p.R178W	7 (HOM, M, P)	*C. reinhardtii*						
A2338–21							7 yr	SRNS	7 yr	First transplant (10 yr)	GS (7 yr)	NA
A2338–22							13 yr	SRNS	ND	First transplant (15 yr)	FSGS (13 yr)	NA
231	Algerian	No	c.645delT	p.F215Lfs*14	8 (het, P)	NA						
			c.1430G>A	p.R477Q	15 (het, M)	*C. reinhardtii*						
231–21							13 yr	SRNS	13 yr	First transplant (15 yr)	FSGS (15 yr)	NA
231–22							12 yr	SRNS	12 yr	First transplant (13 yr)	FSGS (13 yr)	NA
A5170	ND	No	c.857A>G	p.D286G	10 (het, P)	*C. reinhardtii*						
			c.1447G>T	p.E483*	15 (het, M)	NA						
A5170–21							14 yr	SRNS	15 yr	CsA; first transplant (18 yr)	FSGS (15 yr)	HT, goiter
A5170–22							3 yr	SRNS	ND	ND	FSGS (13 yr)	ND
A5170–23							9 yr	SRNS	ND	ACE-I	FSGS (11 yr)	ND
ABD	Tunisian	Yes	c.958C>T	p.R320W	11 (HOM, M, P)	*C. reinhardtii*						
ABD–21							12 yr	SRNS	17 yr	ACE-I; first transplant (17 yr)	FSGS (12 yr)	Goiter
ABD–22							20 yr	SRNS	23 yr	No treatment (discovered in ESKD)	ND	ND
Mek	Moroccan	Yes	c.1027C>T	p.R343W	11 (HOM, M, P)	*C. reinhardtii*						
Mek–1145							20 yr	SRNS	20 yr	ND	ND	DCM
Mek–1146							18 yr	SRNS	19 yr	PNL	cFSGS (19 yr)	ND
A4169	Turkish	Yes	c.1199-1200insA	p.H400Nfs*11	13 (HOM, M, P)	NA						
A4169–21							<1 yr	SRNS	ND	PNL, ACE-I, CP-R, CoQ_{10}[B]	FSGS (5 yr)	Neurologic developmental delay
	Indian	Yes	c.1356_1362del	p.Q452Hfs	15 (HOM, M, P)	NA						
Pt5496			GGGCCCT				16 yr	SRNS		CsA, ACE-I	cFSGS (18 yr)	ND
Pt5497							21 yr	SRNS		ACE-I	cFSGS (22 yr)	ND

[A]All mutations were absent from >60 ethnically matched healthy control individuals and from >8,600 European controls in the Exome Variant Server. [B]Treatment-sensitive case. ACE-I, ACE inhibitor; CoQ_{10}, treatment with CoQ_{10}; CP-R, cyclophosphamide resistant; CsA, cyclosporine A; DCM, dilated cardiomyopathy; GS, global glomerulosclerosis; het, heterozygous in affected individual; HOM, homozygous in affected individual; HT, hypertension; M, heterozygous mutation identified in mother; NA, not applicable; ND, no data or DNA available; P, heterozygous mutation identified in father; PNL, prednisolone.

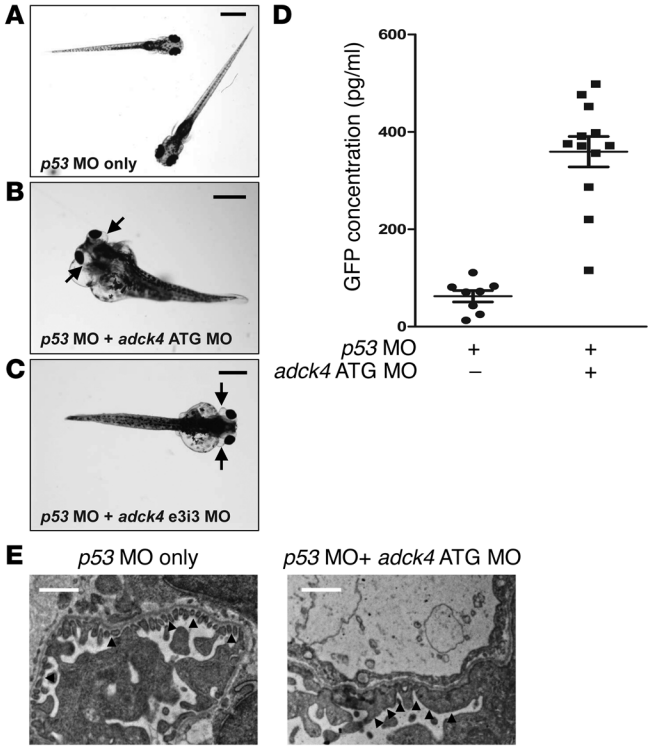

Figure 2
Functional analysis of *adck4* knockdown in zebrafish. (**A**) Control zebrafish were injected with *p53* MO (0.2 mM) as a control to minimize nonspecific MO effects. *p53* MO was injected into fertilized eggs at the 1- to 4-cells stage and did not produce any phenotype up to 168 hpf (n >100). Scale bar: 0.5 mm. (**B**) Zebrafish coinjected with *adck4* ATG MO (0.2 mM) targeting the translation initiation site of zebrafish *adck4* and with *p53* MO. At 120 hpf, *adck4* morphants display the nephrosis phenotype of periorbital edema (arrows) and total body edema in 54.1% (193 out of 357) of embryos. (**C**) Zebrafish coinjected with *adck4* e3i3 MO (0.2 mM) targeting the donor site of intron 3 of zebrafish *adck4* and with *p53* MO. At 120 hpf, *adck4* morphants display the nephrosis phenotype (arrows) in 48.3% (274 out of 567) of embryos. Scale bar: 1 mm (**B** and **C**). (**D**) Proteinuria assay by ELISA against a fusion protein of vitamin D–binding protein and GFP in *l-fabp*::VDBP-GFP transgenic zebrafish. Note that knockdown of *adck4* causes significant proteinuria compared with that in control fish injected with p53 MO only. (P < 0.001). Symbols indicate each measurements; horizontal bars indicate the average; data are presented with the average ± SEM denoted by 3 horizontal lines. (**E**) Electron microscopic ultrastructure of GBM and podocyte foot processes in *p53* MO control and *adck4* morphant zebrafish. In the control zebrafish, the foot processes are regularly spanned by slit diaphragms (black arrowheads). In contrast, the foot processes of the morphants are effaced and disorganized (black arrowheads). Scale bar: 2 μm.

amino acids) (Figure 1E). Analysis of the ADCK4 amino acid sequence yielded a helical domain and an ABC1 domain and a kinase domain (Figure 1E). ADCK4 has high sequence similarity to Abc1/Coq8 and is evolutionarily conserved to *Ciona intestinalis* (sea squirt) (XP_002126787.1), *Drosophila melanogaster* (NP_572836.1), *Caenorhabditis elegans* (NP_498014.2), *C. reinhardtii* (XP_001702520.1), and *Saccharomyces cerevisiae* (NP_011396.1), suggesting a conserved function of the domain assembly.

Knockdown of adck4 in animal models recapitulates the nephrosis phenotype. To further validate the causative role of *ADCK4* for the SRNS phenotype, we performed knockdown of the *ADCK4* ortholog in zebrafish. For zebrafish gene knockdown experiments, we used a *p53* morpholino oligonucleotide (MO) as a negative control to minimize nonspecific apoptotic MO effects (11). *p53* MO injection into fertilized zebrafish eggs at the 1- to 4-cell stage did not produce any phenotype through 168 hours postfertilization (hpf) (Figure 2A). However, coinjection of the *p53* control MO with an MO targeting the translation initiation site of zebrafish *adck4* caused the nephrosis phenotype of periorbital and total body edema, reminiscent of signs of NS in humans, in 54.1% of embryos at 120 hpf (Figure 2B). Similar results were obtained with 2 MOs targeting the splice donor site (e2i2 MO and e3i3 MO) (Figure 2C; Supplemental Figure 1, A–D; and Supplemental Table 3). The summary of edema phenotype observed in *adck4* morphants is displayed in Supplemental Figure 1E. The proteinuric effect of the *adck4* MO was confirmed using an established zebrafish proteinuria assay (12) by ELISA against a fusion protein of vitamin D–binding protein and GFP in *l-fabp*::VDBP-GFP transgenic zebrafish (Figure 2D). We then performed transmission electron microscopy imaging of zebrafish to permit a more direct evaluation of glomerular structures of morphants. When compared with the control (Figure 2E), we observed upon knockdown of *adck4* characteristic alterations of nephrosis (Figure 2E). These included podocyte foot process effacement and disorganization, rarefaction of slit membranes, and disorganization of the glomerular basement membranes in zebrafish glomeruli (Figure 2E, black arrowheads in right panel), as previously described in *plce1* knockdown (13).

In addition, we performed knockdown of *Drosophila coq8* (*dcoq8*) in *Drosophila* pericardial nephrocytes, which share remarkable similarities to the glomerular podocytes (14). The protein uptake assay showed that knockdown of *dcoq8* in nephrocytes reduced the uptake ability of a secreted fusion protein of rat atrial natriuretic factor (ANF) and GFP, suggesting that *dcoq8* is required for nephrocyte function in *Drosophila* (Supplemental Figure 2, A and B). The amino acid of dCoq8 has 53% sequence identity to both ADCK3 and ADCK4 *Drosophila* (Supplemental Figure 2C).

ADCK4 localizes to the mitochondria and foot processes in podocytes. Since most gene products that are defective in SRNS are located in glomerular podocytes, we examined the subcellular localization of ADCK4 in adult rat kidney by immunofluorescence (IF). Podocytes, as identified by expression of nuclear WT1, expressed ADCK4 at high levels in cell bodies and primary processes (Figure 3A). ADCK4 also partially colocalized with cytochrome oxidase subunit VI (COXIV) and mitochondrially encoded cytochrome c oxidase 1 (MTCO1), 2 known mitochondrial marker proteins, suggesting that ADCK4 partly localizes to the mitochondria in renal glomeruli (Figure 3, B and C). In addition, ADCK4 is detected in proximal tubules and collecting ducts (Supplemental Figure 3, A and B). To further investigate the localization of ADCK4, we performed immunogold electron microscopy in adult rat kidneys. In podocytes, ADCK4 was predominantly detected at foot processes (Figure 3D). The specificity of the anti-ADCK4 antibody used in the IF and immunogold electron microscopy studies is demonstrated in Supplemental Figure 4. We also examined the

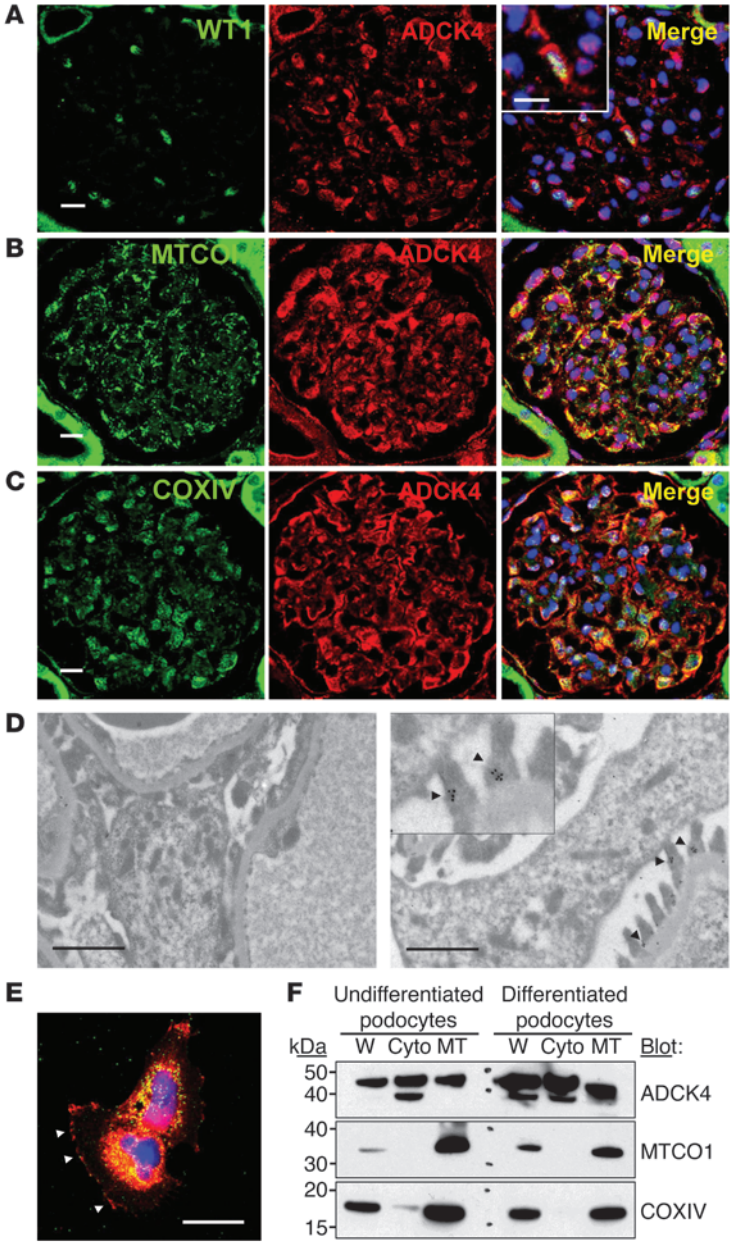

Figure 3
ADCK4 localizes to the mitochondria and cytoplasm of podocytes in adult rat glomeruli and also in cultured human podocytes. (**A**–**C**) Coimmunofluorescence of ADCK4 with (**A**) WT1 as well as (**B**) MTCO1 and (**C**) COXIV in adult rat glomeruli. ADCK4 partially colocalizes to mitochondria with the 2 mitochondrial markers COXIV and MTCO1. Scale bar: 10 μm. (**D**) Immunogold electron microscopy of adult rat kidney displays localization of ADCK4 (black arrowheads) at podocyte foot processes of glomeruli. A control without a primary antibody is shown on the left. Scale bar: 1 μm; ×2.5 (inset). (**E**) Podocytes were transfected with ADCK4-RFP and stained with an anti-COXIV antibody. ADCK4 partially colocalizes to mitochondria with COXIV. Note that ADCK4 also localizes along the plasma membrane (white arrowheads) in podocytes. Scale bar: 25 μm. (**F**) Subcellular fractionation of ADCK4 in undifferentiated and differentiated podocytes. Mitochondrial and cytosol fractions were prepared and immunoblotted for ADCK4, MTCO1, and COXIV, respectively. Each lane was loaded with 50 μg protein. Note that ADCK4 is present in both mitochondrial (marked by MTCO1 and COXIV), and cytosolic fractions in both undifferentiated and differentiated podocytes. W, whole cell lysates; Cyto, cytosol fraction; MT, mitochondrial fraction.

expression of ADCK4 in cultured podocytes by IF. The overexpressed ADCK4–red fluorescent protein (ADCK4-RFP) partially colocalized to mitochondria, and we also noticed that ADCK4-RFP localized to ruffles (Figure 3E) of podocytes, the equivalents of foot processes (Figure 3E and Supplemental Figure 3, C and D). Consistent with data from the cellular fractionation of cultured podocytes, these findings showed that ADCK4 is endogenously present in both the cytosolic and mitochondrial fractions (Figure 3F). Thus, in addition to its role in the mitochondrial respiratory chain, ADCK4 seems to have a very localized function at ruffles and foot processes of podocytes.

ADCK4 is enriched in podocytes and interacts with COQ6 and COQ7. By quantitative real-time PCR, we showed that, although ADCK3 expression exceeds that of ADCK4 in most human tissues (Supplemental Figure 5), ADCK4 is enriched in both differentiated and undifferentiated human podocytes (Figure 4A).

Furthermore, we performed coimmunoprecipitation studies in cultured podocytes to examine whether ADCK4 interacts with other proteins like COQ6 and COQ7 that are involved in the coenzyme Q_{10} (CoQ_{10}) biosynthesis pathway. COQ6 was overexpressed in podocytes, and coimmunoprecipitation was performed. Interestingly, the protein complex precipitated by COQ6 included COQ7 and ADCK4 (Figure 4B). We also confirmed that ADCK4 and COQ6 interact endogenously in lysates from differentiated podocytes (Figure 4C).

Levels of CoQ_{10} are decreased in individuals with ADCK4 mutations. To investigate whether the defect in *ADCK4* has any effect on CoQ_{10} biosynthesis, we measured the total CoQ_{10} contents in EBV-transformed lymphoblasts or cultured skin fibroblasts derived from individuals from the A2338, A4169, and Pt5496/Pt5497 families, in which *ADCK4* mutations were detected. In the case of the A2338 and A4169 families, the total CoQ_{10} was found to be strongly reduced in the affected siblings, A2338-21 (81.92 ± 18.45 pmol/mg protein) and A2338-22 (75.99 ± 34.60 pmol/mg protein), who have a homozygous missense mutation (p.R178W), and in an affected individual, A4169-21 (59.12 ± 9.57 pmol/mg protein), who has a homozygous frameshift mutation (p.H400Nfs*11) (Figure 5A). In contrast, the unaffected individuals, A2338-26 and A2338-27, who have both wild-type alleles, had 784.40 ± 164.10 and 758.00 ± 286.60 pmol/mg protein of total CoQ_{10}, respectively (Figure 5A).

Likewise, in the case of Pt5496 and Pt5497, we confirmed similar results and found that the total CoQ_{10} was reduced in fibroblasts (20.11 ± 3.41 pmol/mg protein for #50552 and 19.75 ± 4.63 pmol/mg protein for #50553) from these individuals, who have a homozygous frameshift mutation (p.Q452Hfs), and normal in fibroblasts (64.33 ± 11.92 pmol/mg protein for #50551 and 83.04 ± 20.64 pmol/mg protein for #50550) from the unaffected parents (Figure 5B).

In addition, we examined mitochondrial respiratory enzyme activity in fibroblasts by measuring maximal uncoupled oxygen

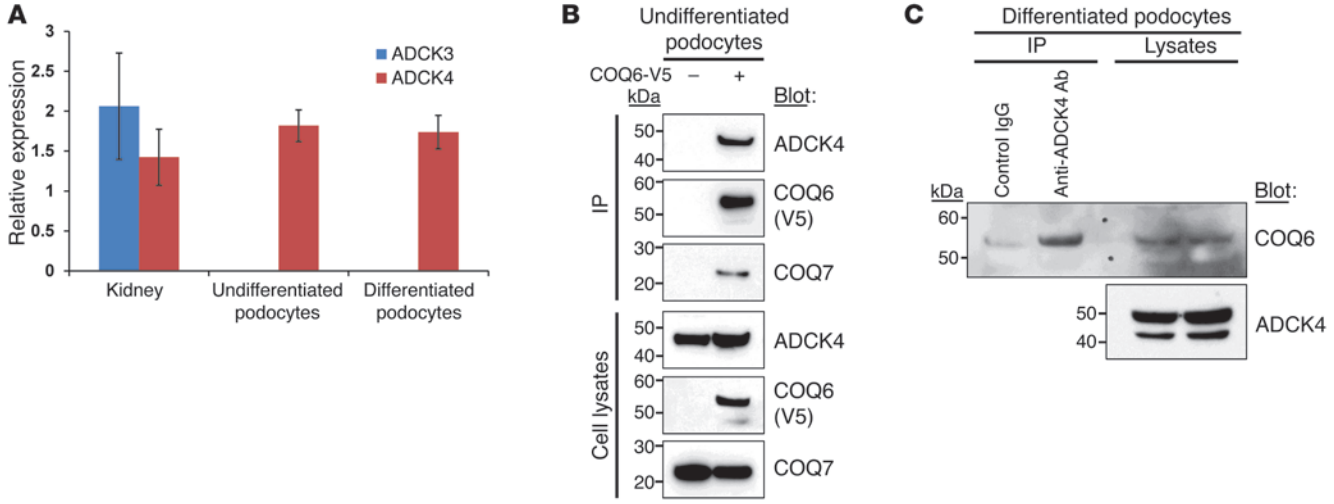

Figure 4

ADCK4 is enriched in podocytes and interacts with COQ6 and COQ7. (**A**) Relative expression of ADCK3 and ADCK4 in kidney tissue and podocytes, as measured by quantitative real-time PCR. Error bars indicate SD of 4 experiments. (**B**) Interaction of ADCK4 with COQ6 and COQ7 in cultured human podocytes. A C-terminally V5-tagged COQ6 construct (COQ6-V6) was transfected into the undifferentiated cultured podocytes. Coimmunoprecipitation was performed using an anti-V5 antibody and then blotting was performed with antibodies for ADCK4, COQ6, and COQ7. Note that the protein complex precipitated by COQ6 includes COQ7 and ADCK4. (**C**) Interaction of endogenous ADCK4 and COQ6 in differentiated podocytes. Podocyte lysates were precipitated with an anti-ADCK4 antibody or a control rabbit IgG. The precipitated proteins were separated by SDS-PAGE and blotted with an anti-COQ6 antibody.

consumption rate (OCR), which shows the CoQ_{10} transfer of electrons from mitochondrial complex I and complex II to complex III. Maximal OCR was significantly reduced in fibroblasts from Pt5496 and Pt5497 compared with that in fibroblasts from controls or their healthy parents (Figure 5C).

Loss of ADCK4 does not induce proliferation or apoptosis in fibroblasts or cultured podocytes. We had previously reported that knockdown of COQ6 can cause apoptosis in podocytes (7). Since ADCK4 interacts with COQ6, we investigated the effect of loss of ADCK4 on cell proliferation and apoptosis in fibroblasts from individuals with a homozygous frameshift ADCK4 mutation (Pt5496 and Pt5497) and their healthy parents as well as in cultured podocytes. We found that fibroblasts (#50552 and #50553) from affected individuals did not show any difference in cell proliferation or apoptosis induced by hydrogen peroxide compared to parental fibroblasts (#50550 and #50551) (Supplemental Figure 6, A and B). Furthermore, in contrast to COQ6, knockdown of *ADCK4* in podocytes did not affect proliferation or apoptosis (Supplemental Figure 6, C and D).

ADCK4 knockdown reduces podocyte migration, which is reversed by the addition of CoQ_{10}. We next examined the effect of ADCK4 knockdown on podocyte migration using the xCELLigence system, which monitors cell migration in real-time (Figure 6). We found that migration of podocytes was reduced by knockdown of ADCK4 (Figure 6A). Because CoQ_{10} treatment had resulted in improvement of the NS phenotype in an individual with a mutation in *ADCK4*, we tested the effect of the addition of CoQ_{10} on podocyte migration. Interestingly, we found that the addition of CoQ_{10} reversed the decreased migratory phenotype caused by ADCK4 knockdown (Figure 6, A and B). Similar results were obtained when 2 additional siRNAs were used for knockdown of ADCK4 in cultured human podocytes (*ADCK4* siRNAs #5 and #6) (Figure 6, C and D). We further found that decreased migration, which was caused by an *ADCK4* siRNA (*ADCK4* siRNA #6), was reversed when wild-type mouse ADCK4 was transfected into podocytes (Figure 6C). This result also confirmed that the effect on podocyte migration was caused by *ADCK4* loss of function.

Discussion

Here, we describe the discovery of mutations in *ADCK4* as causes of SRNS. We have shown that ADCK4 is expressed in podocytes and localizes to mitochondria and foot processes and interacts with COQ6 endogenously. Knockdown of ADCK4 in podocytes reduced their migration phenotype, which could be reversed by overexpression of siRNA-resistant ADCK4 or, most importantly, by the addition of CoQ_{10}. By knockdown of *adck4* in zebrafish, we clearly demonstrated that the function of this gene is necessary to avoid the NS disease phenotype. The fact that ADCK4 has high sequence similarity with ADCK3, which was previously reported to be associated with CoQ_{10} deficiency (15), and the fact that cells from affected individuals with *ADCK4* mutations (families A2338, A4169, and Pt5496/Pt5497) had reduced total CoQ_{10} content suggests that ADCK4 is also involved in CoQ_{10} biosynthesis.

CoQ_{10}, also known as ubiquinone, is a lipid-soluble component of virtually all cell membranes, in which it is thought to play an important antioxidant role as well as to transport electrons from complexes I and II to complex III in the respiratory chain of the mitochondrial inner membrane (16). The biochemical pathway of CoQ_{10} biosynthesis is complex and has not been completely elucidated. Primary CoQ_{10} deficiencies due to mutations in ubiquinone biosynthetic genes (*COQ2*, *COQ4*, *COQ6*, *PDSS1*, *PDSS2*, and *ADCK3*) have been identified (7, 15, 17–26). Clinical manifestations of CoQ_{10} deficiency are variable. For example, individuals with *COQ2* mutations present with phenotypes ranging from isolated NS to catastrophic neonatal multisystem disorder with encephalomyopathy and renal involvement to a recently described multiple-system atrophy (20, 23–27). In

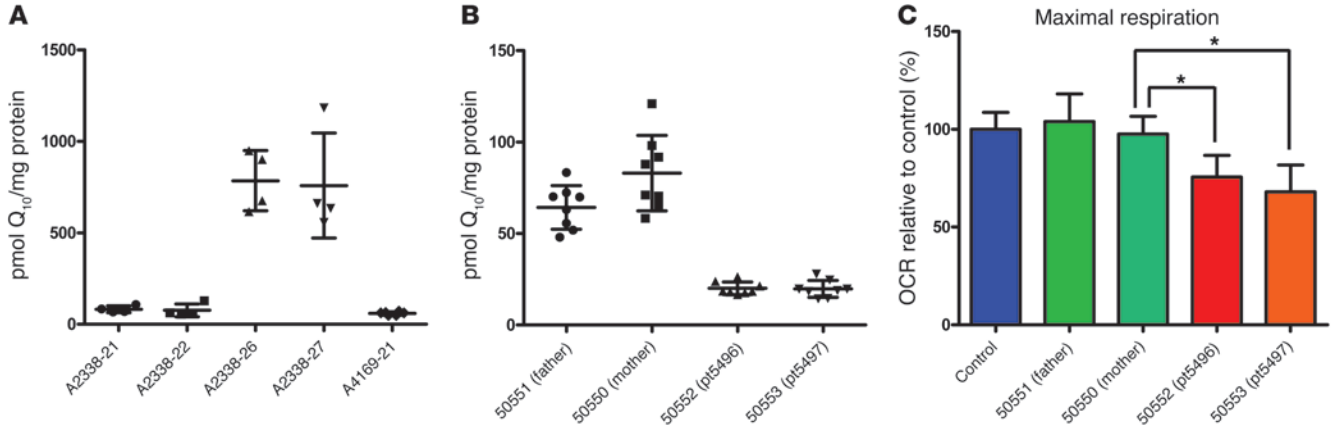

Figure 5

CoQ_{10} content in EBV-transformed lymphoblasts and fibroblasts from SRNS families with mutations in *ADCK4*. (**A**) Scatter plot showing the total CoQ_{10} content in EBV-transformed lymphoblasts derived from either healthy or affected individuals from the A2338 and A4169 families. Individuals A2338-21, A2338-22, and A4169-21 are affected with SRNS, while A2338-26 and A2338-27 have both wild-type alleles. The content of CoQ_{10} is presented with the average ± SD denoted by 3 horizontal lines ($n = 4$; except $n = 6$ for A4169-21). The content from A2338-26 is significantly higher than the CoQ10 content from A2338-21, A2338-22, and A4169-21 (multiple comparison, $P < 0.0001$). Symbols indicate individual lymphoblasts; horizontal bars indicate the average. (**B**) Scatter plot showing the total CoQ_{10} content in fibroblasts derived from either healthy parents or affected individuals (Pt5496 and Pt5497). The content of CoQ_{10} is presented with the average ± SD denoted by 3 horizontal lines ($n = 8$). CoQ_{10} content from #50551 is statistically lower than CoQ_{10} content from #50550 (multiple comparison, $P = 0.0134$) and significantly higher than the CoQ_{10} contents from #50552 and #50553 (multiple comparison, $P < 0.0001$). Symbols indicate individual fibroblasts; horizontal bars indicate the average. (**C**) In vivo maximal uncoupled OCR over the whole respiratory chain, including the Q_{10} transfer of electrons from mitochondrial complex I and complex II to complex III. Maximal respiration was significantly reduced in fibroblasts from Pt5496 and Pt5497 compared with that in control fibroblasts. Data shown are mean ± SD ($n > 10$). *$P < 0.001$.

addition, *COQ6* (7) and *PDSS2* (19) have also been implicated in the cause of SRNS.

We as well as Montini et al. have shown previously that the individuals affected with SRNS due to mutations in CoQ_{10} biosynthesis pathway genes like *COQ2* and *COQ6* can be treated with the innocuous food supplement CoQ_{10} (7, 28). CoQ_{10} deficiency in individuals with *ADCK4* mutations thus raises the possibility of supplementation therapy. So far, only one individual (A4169-21) with *ADCK4* mutation has been treated with CoQ_{10} (15 mg/kg/d) for over 4 years. He was first treated with intravenous methylprednisolone followed by 2 mg/kg/d prednisolone over 10 weeks without achieving remission of NS. Subsequently, he was treated with 2 mg/kg/d cyclophosphamide for 3 months. The treatment resulted in partial remission, but treatment had to be stopped because of infections. Treatment with CoQ_{10} was commenced at 1 year of age, giving 100 mg/d CoQ_{10} orally together with 5 mg of prednisolone every other day. Then, the edema disappeared and proteinuria decreased significantly. The individual is currently being treated with CoQ_{10} (15 mg/kg/d) with captopril (12.5 mg/d). Even though the effectiveness of CoQ_{10} treatment cannot be generalized for individuals with *ADCK4* mutations at the moment based on this single case, we still think that the identification of molecular defects of CoQ_{10} biosynthesis is important because they may represent forms of SRNS that are treatable by administration of CoQ_{10}.

ADCK3 and ADCK4 are highly similar members of an ancient atypical kinase family and appear to result from gene duplication in vertebrates (15). The yeast Coq8/Abc1 is required for CoQ biosynthesis (29) and is essential for the organization of high-molecular-mass Coq polypeptide complex and for phosphorylated forms of the Coq3, Coq5, and Coq7 polypeptides that perform methylation and hydroxylation steps in CoQ biosynthesis (30, 31). Considering their similarity, it is interesting that mutations in *ADCK3* result in cerebellar ataxia and seizures without renal involvement (15, 21), whereas mutations in *ADCK4* cause SRNS mostly without neurological symptoms. Currently, there is no clear explanation for this; however, this may be partially due to their differential tissue expression (Figure 4A and Supplemental Figure 5). Xie et al. previously showed that ADCK3 can rescue yeast *coq8* mutants and restore phosphorylated forms of yeast Coq polypeptides (30), but the same group observed that expression of ADCK4 failed to rescue *coq8* mutants (data not shown). On the other hand, knockdown of *Dcoq8*, which has 53% amino acid identity to both ADCK3 and ADCK4, caused defects in nephrocyte function (Supplemental Figure 2). Overall, these results suggest that ADCK3 and ADCK4 are independently required for synthesis of CoQ, yet retain distinct functions, a difference that may have evolved in vertebrates, and that ADCK3 may be closer to yeast Coq8.

cFSGS is defined morphologically by the presence of hyperplastic and hypertropic podocytes overlying collapsed capillary loops within glomerular tufts (32). Interestingly, the histology of affected individuals (1146, Pt5496, and Pt5497) with *ADCK4* mutations showed cFSGS. In addition, mutant *kd/kd* mice, which have a missense mutation in *Pdss2* and present with isolated nephropathy, have features of cFSGS (33). Therefore, it will be important to investigate whether nephropathy resulting from CoQ_{10} deficiency results in cFSGS, because this may be a phenotypic criterion with which to choose individuals with SRNS that should be screened for genes involved in CoQ_{10} biosynthesis, such as *COQ2*, *COQ6*, *PDSS2*, and *ADCK4*. To answer this, it is necessary to investigate more SRNS cases resulting from CoQ_{10} deficiency. In addition, knockout animal models for *Coq2*, *Coq6*, and *Adck4* will be helpful.

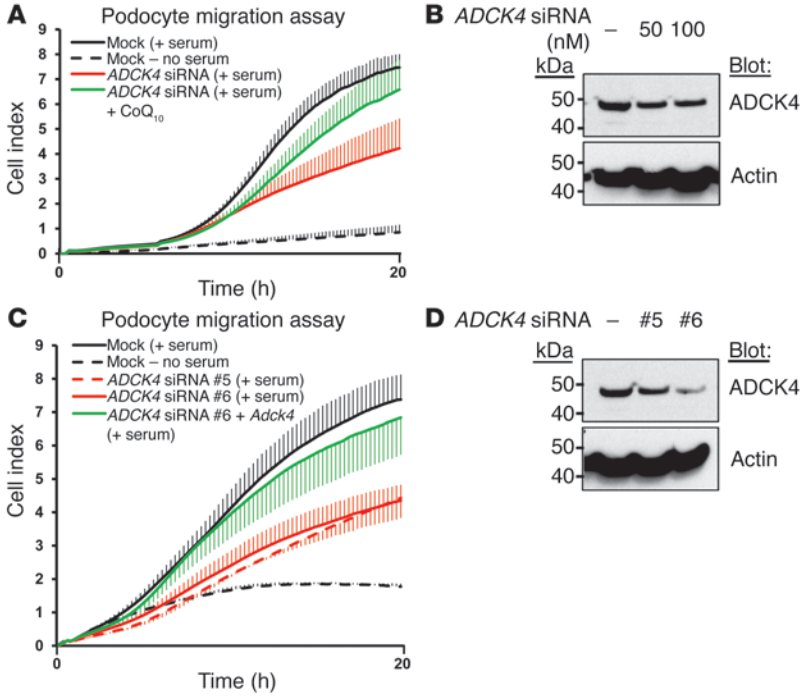

Figure 6
Knockdown of ADCK4 decreases the migratory phenotype of podocytes. (**A**) The effect of ADCK4 knockdown on podocyte migration. Podocytes transfected with *ADCK4* siRNA (red) exhibited decreased migration compared with podocytes transfected with scrambled siRNA (black). The decrease in podocyte migration was partially reversed by the addition of 50 μM CoQ_{10} (green). Error bars are shown in only one direction for clarity and indicate SDs from 3 independent experiments. (**B**) The efficiency of *ADCK4* siRNA used in **A** was confirmed by immunoblotting with an anti-ADCK4 antibody and an anti–β-actin antibody. (**C**) Transfection of podocytes with 2 additional *ADCK4*-specific siRNAs (siRNA #5 and #6) confirmed the result from **A** that ADCK4 knockdown in human podocytes reduces migration (red dotted and solid lines) compared with podocytes transfected with the scrambled siRNA (black). The decrease in podocyte migration by ADCK4 knockdown using *ADCK4* siRNA #6 was rescued by transfection of mouse *Adck4* construct (green). Mouse ADCK4 has 5 mismatches from the siRNA target sequences. Error bars indicate SDs of 3 independent experiments. (**D**) The efficiency of *ADCK4* siRNAs used in **C** was confirmed by immunoblotting. 100 nM of each siRNA was transfected into podocytes.

In conclusion, we identified recessive mutations in *ADCK4* as novel single-gene causes of SRNS. Early recognition of this new genetic entity of SRNS will be important because it may represent a form of SRNS that can potentially be treated by CoQ_{10} supplementation.

Methods

Subjects. Following informed consent, we obtained clinical data and blood samples from individuals with SRNS or steroid-sensitive NS from worldwide sources. The diagnosis of NS was made by (pediatric) nephrologists based on standardized clinical and renal histological criteria (34). Renal biopsies were evaluated by renal pathologists. Clinical data were obtained using a standardized questionnaire (http://www.renalgenes.org).

HM, WER, and mutation calling. For the A2338 family, HM, WER, and mutation calling were performed as described previously (35). HM in the 231 and ABD families was performed using Human Mapping 250k *NspI* Array (Affymetrix), and parametric logarithm of odds (LOD) scores were calculated with MERLIN (36). For WER of the 231, ABD, and Mek families, DNA was processed using All Exon 50Mb V3 (Agilent SureSelect) to enrich for exonic sequences and a SOLiD 5500XL high-throughput sequencing machine (Applied Biosystems) (paired-end reads: 50 bases forward, 25 bases reverse). Obtained sequences were aligned to the human genome (NCBI build 37/hg19) using Lifescope suite from Lifetech. Substitution and variation calls were made with the GATK pipeline (mpileup, bfctools, vcfuitil). Variants were then annotated with an in-house software (Polyweb), which allows users to set up bioinformatic filters in order to identify the putative mutation.

Plasmids, cell culture, and transfection. A human *ADCK4* clone was purchased from Open Biosystems (clone accession BC013114.1). The mutant clones of *ADCK4* were generated by a PCR-based site-directed mutagenesis method. The *COQ6* clones were described previously (7). The immortalized human podocytes (37) were maintained in RPMI plus GlutaMAX-I (Gibco) supplemented with 10% FBS, penicillin (50 IU/ml)/streptomycin (50 μg/ml), and Insulin-Transferrin-Selenium-X (Invitrogen). Plasmids and siRNA were transfected into podocytes using Lipofectamine 2000 (Invitrogen). The *ADCK4*-specific and control scrambled siRNAs were purchased from Dharmacon or Sigma-Aldrich. Lymphoblasts were purified from blood samples using Ficoll-Paque PLUS (GE Healthcare) according to the manufacturer's instructions. The isolated lymphoblasts were transformed by EBV and immortalized as described previously (38). Human fibroblasts were grown in DMEM supplemented with 15% FBS, penicillin (50 IU/ml)/streptomycin (50 μg/ml), and nonessential amino acids (Invitrogen).

Immunoblotting, immunoprecipitation, and IF staining. These experiments were performed as described previously (13). Anti-ADCK4 (LSBio), anti-MTCO1 (Abcam), anti-COXIV (Abcam), anti-COQ6 (Santa Cruz Biotechnology Inc.), anti-COQ7 (Proteintech), and anti-V5 (Invitrogen) were used. Fluorescent images were obtained with a Leica SP5X laser scanning microscope.

Immunogold electron microscopy. Rat renal cortex samples were dissected and trimmed into 1-mm-thick blocks, which were fixed by immersion in 4% formaldehyde and 0.5% glutaraldehyde in 0.1 M cacodylate buffer, pH 7.4, and processed for embedment in LR White. Semithin sections (700 nm) were first obtained to locate areas that contained glomeruli. Subsequently, ultrathin sections (70 nm) were obtained from those areas and collected on formvar-coated nickel grids and etched with saturated sodium periodate for 15 minutes. Sections were blocked with 0.1 M phosphate buffer, pH 7.4, containing 1% BSA, 3% goat serum, and 0.05% Tween-20 for 1 hour at room temperature and incubated with a rabbit anti-ADCK4 antibody (LSBio) in buffer overnight at 4°C. Sections were then washed and incubated with goat anti-rabbit IgG conjugated to 18 nm gold (Jackson ImmunoResearch Laboratories) and stained with uranyl acetate. Sections in which the primary antibody was omitted during the overnight incubation were used as negative control. Sections were observed on a Zeiss 910 transmission electron microscope.

Mitochondrial fractionation. The mitochondrial fractionation of podocytes was done using Mitochondrial Isolation Kit for Cultured Cells (Thermo Scientific), Mitochondrial/Cytosol Fractionation Kit (Abcam), and Mitochondrial Fractionation Kit (Active Motif) according to the manufacturer's instructions.

Podocyte migration and proliferation assay. Real-time migration assays were performed using the xCELLIgence system (ACEA Biosciences) according to the manufacturer's instructions. For migration assays, 24 hours after transfection, 4×10^4 cells were plated with serum-free media in the upper chamber of the CIM-plate 16 (ACEA Biosciences). The lower chambers were filled with 10% FBS for chemoattraction or with serum-free media. For proliferation assays, 4×10^4 cells were plated with serum-free media in the E-plate 16 (ACEA Biosciences). The data obtained were analyzed with RTCA software. Results are presented as the time versus cell index curve.

Zebrafish studies. Zebrafish (*Danio rerio*) were maintained and reared as described previously (12). Approval for zebrafish research was obtained from the University of Michigan and the Boston Children's Hospital Committees on the Use and Care of Animals. MOs were injected into the AB* wild-type strain for phenotype analysis of morphants and transmission electron microscopy. The proteinuria assays were performed using *l-fabp*::VDBP-GFP transgenic fish and the GFP ELISA Kit (Cell Biolabs) as described previously (12).

CoQ_{10} measurements. Cells (approximately 0.1 g) were thawed on ice and resuspended in 1.5 ml phosphate-buffered saline (0.14 M NaCl, 12.0 mM NaH_2PO_4, 8.1 mM Na_2HPO_4, pH 7.4), followed by homogenization with a polytron (Kinematica PT 2500E) for 1 minute at 15,300 *g* on ice. Lipid extracts were prepared by addition of 1.2 ml methanol, followed by 1.8 ml petroleum ether. Diethoxy-CoQ_{10} served as an internal standard (39). A typical standard curve contains 5 standards with 7.2 pmol, 20 pmol, 72 pmol, 140 pmol, and 400 pmol of CoQ_{10}, respectively. Standard curve samples and experimental samples shared identical extractions. Each of the extraction tubes were vortexed for 45 seconds. The upper layer was removed, and the lower aqueous phase was reextracted with 1.8 ml petroleum ether. Nitrogen gas dried the combined organic phase, and 200 μl ethanol dissolved the dried lipids (USP, Apaer Alcohol and Chemical Co.). A binary HPLC solvent delivery system with a Luna Phenyl-Hexyl column (particle size 3 μm, 50 × 2.00 mm; Phenomenex) coupled with an Applied Biosystems 4000 QTRAP linear MS/MS spectrometer determined the total CoQ_{10} content. The mobile phase consisted of solvent A (methanol/isopropanol, 95:5, with 2.5 mM ammonium formate) and solvent B (isopropanol, with 2.5 mM ammonium formate). The percentage of solvent B started at 0% for the first 1.5 minutes, increased linearly to 15% by 2 minutes, remained constant for the next 1 minute, and decreased linearly back to 0% by 4 minutes. The flow rate remained constant at 600 μl/min. Data acquisition and processing required Analyst software (version 1.4.2). Multiple-reaction monitoring mode detected quinone content, with the following transitions: mass-to-charge [*m*/*z*] ratio 880.7:197.0 (CoQ_{10} with ammonium adduct); *m*/*z* 882.7:197.0 ($Q_{10}H_2$ with ammonium adduct); *m*/*z* 908.7:225.1 (diethoxy-Q_{10} with ammonium adduct), and *m*/*z* 910.7:225.1 (diethoxy-$Q_{10}H_2$ with ammonium adduct).

Mitochondrial respiratory enzyme activity measurement. Fibroblasts derived from controls (NHDF-neo, Bio-Rad), healthy parents, or 2 affected individuals (Pt5496 and Pt5497) were seeded at 20,000 cells per well in 80 ml DMEM and incubated at 37°C, 5% CO_2 for 24 hours. In vivo maximal uncoupled OCR over the whole respiratory chain, including the CoQ_{10} transfer of electrons from mitochondrial complex I and complex II to complex III, was measured using the XF96 Extracellular Flux Analyzer (Seahorse Bioscience) (40). Mitochondria membrane potential was uncoupled by the addition of carbonyl cyanide 4-(trifluoromethoxy) phenylhydrazone (FCCP, 0.4 μM). Nonmitochondrial respiration was determined after the addition of 2.5 μM rotenone/5 μM antimycin A.

RNAi-based Drosophila nephrocyte functional assay. The MHC-ANF-RFP transgenic flies were generated in previous studies (14, 41). Nephrocyte-specific gene knockdown was achieved by using nephrocyte-specific Gal4 and UAS-RNAi transgenes (14, 41). Nephrocyte function was measured by the amount of secreted red fluorescent proteins accumulated in nephrocytes at the second instar larvae stage (14, 41). Hand-GFP (42) was used to label the cardiac nephrocytes.

Statistics. Results are presented as mean ± SEM or SD for the number of experiments indicated in the figure legends. Statistical analysis of continuous data was performed with 2-tailed Student's *t* test or multiple comparison, as appropriate. $P < 0.05$ was considered statistically significant.

Study approval. Approval for research in human subjects was obtained from the IRBs of the University of Michigan, Boston Children's Hospital, Université Paris Descartes, University of Toronto, Yale University, and Beth Israel Deaconess Medical Center.

Acknowledgments

The authors thank the families who contributed to this study. This research was supported by grants from the NIH to F. Hildebrandt (DK076683, DK086542), to R.C. Wiggins (DK46073 and DK081943), to E.A. Otto (DK090917), to W. Zhou (DK091405), to Z. Han (R01HL090801), to D.S. Williams (EY07042), and to R.P. Lifton (U54HG006504); by the Kidney Foundation of Canada and Nephcure Canada (to A.D. Paterson and Y. Pei); by the Nephcure Foundation (to F. Hildebrandt and M. Pollak); by the National Research Foundation (Basic Science Research Program funded by the Ministry of Education, Science and Technology) (to H.Y. Gee, 2012R1A6A3A03040212); by the American Heart Association (to Z. Han, AHA-0630178N); by the Association Francaise contre les Myopathies (to C. Antignac, GLOMGENE project: ANR-08-GENOPAT-017-01); by the Fondation pour la Recherche Médicale (to C. Antignac, project DMP 2010-11-20-386); by the European Community's 7th Framework program grant (to C. Antignac, Eurenomics 2012-305608); by a Ruth L. Kirschstein NIH Service Award (to L.X. Xie, GM 007185); by Kids Kidney Research and Garfield Weston Foundation (to D. Böckenhauer and R. Kleta); by the King Abdul-Aziz University (to J.A. Kari, D. Böckenhauer, and R. Kleta); by the Fondazione CARIPARO (to L. Salviati); by a National Science Foundation grant (to C.F. Clarke, 0919609); and by the German Network of mitochondrial disorders (to H. Prokisch, mitoNET 01GM1113C). The LC-MS/MS determination of quinones was supported in part by NIH grant S10RR024605 from the National Center for Research Resources. The authors also acknowledge with thanks the Deanship of Scientific Research; King Abdulaziz University, Jeddah, for their support; the Bloomington stock center; and the Vienna Drosophila RNAi Center for *Drosophila* stocks. H.Y. Gee is a research fellow of the American Society of Nephrology. A.D. Paterson holds a Canada Research Chair in Complex Traits Genetics. W. Zhou is a Carl W. Gottschalk Scholar. D. Böckenhauer is a Higher Education Funding Council for England Clinical Reader. D.S. Williams is an Research to Prevent Blindness Jules and Doris Stein professor. F. Hildebrandt is an investigator of the Howard Hughes Medical Institute and the Frederick G.L. Huetwell Professor.

Received for publication January 28, 2013, and accepted in revised form September 6, 2013.

Address correspondence to: Friedhelm Hildebrandt, Howard Hughes Medical Institute, Boston Children's Hospital, 300 Longwood Avenue, HU319, Boston, Massachusetts 02115, USA. Phone: 617.355.6129; Fax: 617.730.0569; E-mail: Friedhelm.Hildebrandt@childrens.harvard.edu. Or to: Corinne Antignac, Inserm U983 (ex-U574) and Department of Genetics, Necker Hospital, 149,

rue de Sevres, 75015 Paris, France. Phone: 33.1.44.49.50.98; Fax: 33.1.44.49.02.90; E-mail: corinne.antignac@inserm.fr. Or to: York Pei, Division of Nephrology and of Genomic Medicine, University Health Network and University of Toronto, 8N838, 585 University Avenue, Toronto, Ontario, Canada M5G2N2. Phone: 416.340.4257; Fax: 416.340.4999; E-mail: York.Pei@uhn.ca.

1. Antignac C. Genetic models: clues for understanding the pathogenesis of idiopathic nephrotic syndrome. *J Clin Invest*. 2002;109(4):447–449.
2. Hinkes BG, et al. Nephrotic syndrome in the first year of life: two thirds of cases are caused by mutations in 4 genes (NPHS1, NPHS2, WT1, and LAMB2). *Pediatrics*. 2007;119(4):e907–e919.
3. Kim MS, Stablein D, Harmon WE. Renal transplantation in children with congenital nephrotic syndrome: a report of the North American Pediatric Renal Transplant Cooperative Study (NAPRTCS). *Pediatr Transplant*. 1998;2(4):305–308.
4. Benoit G, Machuca E, Heidet L, Antignac C. Hereditary kidney diseases: highlighting the importance of classical Mendelian phenotypes. *Ann N Y Acad Sci*. 2010;1214:83–98.
5. Hildebrandt F. Genetic kidney diseases. *Lancet*. 2010;375(9722):1287–1295.
6. Ozaltin F, et al. Disruption of PTPRO causes childhood-onset nephrotic syndrome. *Am J Hum Genet*. 2011;89(1):139–147.
7. Heeringa SF, et al. COQ6 mutations in human patients produce nephrotic syndrome with sensorineural deafness. *J Clin Invest*. 2011;121(5):2013–2024.
8. Hildebrandt F, et al. A systematic approach to mapping recessive disease genes in individuals from outbred populations. *PLoS Genet*. 2009; 5(1):e1000353.
9. Otto EA, et al. Candidate exome capture identifies mutation of SDCCAG8 as the cause of a retinal-renal ciliopathy. *Nat Genet*. 2010;42(10):840–850.
10. Halbritter J, et al. High-throughput mutation analysis in patients with a nephronophthisis-associated ciliopathy applying multiplexed barcoded array-based PCR amplification and next-generation sequencing. *J Med Genet*. 2012;49(12):756–767.
11. Robu ME, et al. p53 activation by knockdown technologies. *PLoS Genet*. 2007;3(5):e78.
12. Zhou W, Hildebrandt F. Inducible podocyte injury and proteinuria in transgenic zebrafish. *J Am Soc Nephrol*. 2012;23(6):1039–1047.
13. Hinkes B, et al. Positional cloning uncovers mutations in PLCE1 responsible for a nephrotic syndrome variant that may be reversible. *Nat Genet*. 2006;38(12):1397–1405.
14. Zhang F, Zhao Y, Han Z. An in vivo functional analysis system for renal gene discovery in Drosophila pericardial nephrocytes. *J Am Soc Nephrol*. 2013; 24(2):191–197.
15. Lagier-Tourenne C, et al. ADCK3, an ancestral kinase, is mutated in a form of recessive ataxia associated with coenzyme Q10 deficiency. *Am J Hum Genet*. 2008;82(3):661–672.
16. Quinzii CM, Hirano M. Primary and secondary CoQ_{10} deficiencies in humans. *Biofactors*. 2011; 37(5):361–365.
17. Mollet J, et al. Prenyldiphosphate synthase, subunit 1 (PDSS1) and OH-benzoate polyprenyltransferase (COQ2) mutations in ubiquinone deficiency and oxidative phosphorylation disorders. *J Clin Invest*. 2007;117(3):765–772.
18. Quinzii CM, et al. Coenzyme Q deficiency and cerebellar ataxia associated with an aprataxin mutation. *Neurology*. 2005;64(3):539–541.
19. López LC, et al. Leigh syndrome with nephropathy and CoQ10 deficiency due to decaprenyl diphosphate synthase subunit 2 (PDSS2) mutations. *Am J Hum Genet*. 2006;79(6):1125–1129.
20. Quinzii C, et al. A mutation in para-hydroxybenzoate-polyprenyl transferase (COQ2) causes primary coenzyme Q10 deficiency. *Am J Hum Genet*. 2006; 78(2):345–349.
21. Mollet J, et al. CABC1 gene mutations cause ubiquinone deficiency with cerebellar ataxia and seizures. *Am J Hum Genet*. 2008;82(3):623–630.
22. Salviati L, et al. Haploinsufficiency of COQ4 causes coenzyme Q10 deficiency. *J Med Genet*. 2012; 49(3):187–191.
23. Diomedi-Camassei F, et al. COQ2 nephropathy: a newly described inherited mitochondriopathy with primary renal involvement. *J Am Soc Nephrol*. 2007; 18(10):2773–2780.
24. Lopez-Martin JM, et al. Missense mutation of the COQ2 gene causes defects of bioenergetics and de novo pyrimidine synthesis. *Hum Mol Genet*. 2007; 16(9):1091–1097.
25. McCarthy HJ, et al. Simultaneous sequencing of 24 genes associated with steroid-resistant nephrotic syndrome. *Clin J Am Soc Nephrol*. 2013;8(4):637–648.
26. Salviati L, et al. Infantile encephalomyopathy and nephropathy with CoQ10 deficiency: a CoQ10-responsive condition. *Neurology*. 2005;65(4):606–608.
27. Multiple-System Atrophy Research Collaboration. Mutations in COQ2 in familial and sporadic multiple-system atrophy. *N Engl J Med*. 2013;369(3):233–244.
28. Montini G, Malaventura C, Salviati L. Early coenzyme Q10 supplementation in primary coenzyme Q10 deficiency. *N Engl J Med*. 2008;358(26):2849–2850.
29. Do TQ, Hsu AY, Jonassen T, Lee PT, Clarke CF. A defect in coenzyme Q biosynthesis is responsible for the respiratory deficiency in Saccharomyces cerevisiae abc1 mutants. *J Biol Chem*. 2001; 276(21):18161–18168.
30. Xie LX, et al. Expression of the human atypical kinase ADCK3 rescues coenzyme Q biosynthesis and phosphorylation of Coq polypeptides in yeast coq8 mutants. *Biochim Biophys Acta*. 2011;1811(5):348–360.
31. Tauche A, Krause-Buchholz U, Rödel G. Ubiquinone biosynthesis in Saccharomyces cerevisiae: the molecular organization of O-methylase Coq3p depends on Abc1p/Coq8p. *FEMS Yeast Res*. 2008; 8(8):1263–1275.
32. Albaqumi M, Soos TJ, Barisoni L, Nelson PJ. Collapsing glomerulopathy. *J Am Soc Nephrol*. 2006; 17(10):2854–2863.
33. Barisoni L, Madaio MP, Eraso M, Gasser DL, Nelson PJ. The kd/kd mouse is a model of collapsing glomerulopathy. *J Am Soc Nephrol*. 2005; 16(10):2847–2851.
34. [No authors listed]. Primary nephrotic syndrome in children: Clinical significance of histopathologic variants of minimal change of diffuse mesangial hypercellularity: A Report of the International Study of Kidney Disease in Children. *Kidney Int*. 1981;20(6):765–771.
35. Gee HY, et al. ARHGDIA mutations cause nephrotic syndrome via defective RHO GTPase signaling. *J Clin Invest*. 2013;123(8):3243–3253.
36. Abecasis GR, Cherny SS, Cookson WO, Cardon LR. Merlin--rapid analysis of dense genetic maps using sparse gene flow trees. *Nat Genet*. 2002;30(1):97–101.
37. Saleem MA, et al. A conditionally immortalized human podocyte cell line demonstrating nephrin and podocin expression. *J Am Soc Nephrol*. 2002; 13(3):630–638.
38. Amoli MM, Carthy D, Platt H, Ollier WE. EBV Immortalization of human B lymphocytes separated from small volumes of cryo-preserved whole blood. *Int J Epidemiol*. 2008;37(suppl 1):i41–i45.
39. Falk MJ, et al. Probucol ameliorates renal and metabolic sequelae of primary CoQ deficiency in Pdss2 mutant mice. *EMBO Mol Med*. 2011;3(7):410–427.
40. Haack TB, et al. Molecular diagnosis in mitochondrial complex I deficiency using exome sequencing. *J Med Genet*. 2012;49(4):277–283.
41. Zhang F, Zhao Y, Chao Y, Muir K, Han Z. Cubilin and amnionless mediate protein reabsorption in Drosophila nephrocytes. *J Am Soc Nephrol*. 2013; 24(2):209–216.
42. Han Z, Olson EN. Hand is a direct target of Tinman and GATA factors during Drosophila cardiogenesis and hematopoiesis. *Development*. 2005; 132(15):3525–3536.